σ-Exchange Potential for Nucleon-Nucleon Scattering*

Firooz Partovi† and Earle L. Lomon
Laboratory for Nuclear Science and Department of Physics, Massachusetts Institute of Technology, Cambridge, Massachusetts 02139
(Received 15 November 1971)

A nucleon-nucleon interaction potential is derived which includes all exchanges between a pair of nucleons involving a single σ meson and any number of pion-pair inserts on the σ-meson propagator and vertices. The reduction of the Bethe-Salpeter kernel to a potential follows the method of Partovi and Lomon. The σ-pion and σ-nucleon couplings are restricted by the Adler chiral condition at zero four-momentum transfer, renormalized. The σ-meson mass is taken from experimental evidence to be nearly M_ρ. Various σ-meson widths are considered. Widths greater than 300 MeV predict small σ-meson contributions to the potential due to persistent cancellations between graphs. In particular near the width of about 610 MeV predicted by Weinberg's asymptotic restrictions the σ-potential contribution is a minimum and nearly cancels the familiar one-plus-two nucleon-pair contribution to the potential. The corrections to the previously obtained single-pion, η-, ρ-, and ω-meson and two-pion potentials are such as to increase the resemblance to Hamada-Johnston and Reid potentials or increase the resemblance to the Feshbach-Lomon potential for σ-meson widths near 620 MeV and 660 Mev, respectively.

I. INTRODUCTION

The representation of a relativistic field-theoretical amplitude by a Schrödinger-equation potential has been discussed by Partovi and one of the authors (E.L.L.).[1] An extension of the Blankenbecler-Sugar reduction[2] of the Bethe-Salpeter amplitude to the nucleon-nucleon case and appropriate calculational techniques were shown to lead to an accurate description of the potential generated by single- and multiple-meson exchanges for distances greater than half a pion Compton wavelength. The calculation was made for the one- and two-pion-, and single-η-, -ρ-, and -ω-exchange contributions, using masses and coupling constants as best determined by other than nucleon-nucleon experiments. It was shown that two-pion exchange was very important at intermediate range (0.7–1.5 F). The resultant central and tensor total potentials were quantitatively close to the phenomenological Hamada-Johnston[3] and Reid[4] potentials for all states. The predicted spin-orbit potential did not closely resemble the Hamada-Johnston result, but was qualitatively the same in the better determined isospin $T=1$ case.

In Ref. 1 it was noted that two possibly important corrections to the considered contributions remained to be calculated. Two-pion-exchange graphs with nucleon isobars in the intermediate state had not been considered, nor had exchanges of the $T=0$, $J=0$ σ meson (sometimes called the ϵ meson) been included. The calculation of contributions from all graphs which involve the exchange of a single σ meson and its strong coupling to two pions is the subject of this paper.

We assume the σ meson to be that $T=0$, $J=0$ pion-pion resonance identified to have a mass near 750 MeV.[5] Its width is poorly determined experimentally but is indicated to be in the range of several hundred MeV. The $\sigma\pi\pi$ coupling $g_{\sigma\pi}$ can be determined by the resonance width. There is no experimental information about the $\sigma N\bar{N}$ coupling $g_{\sigma N}$. Current-algebra and chiral-symmetry postulates do determine a value for the product of $g_{\sigma\pi}$ and $g_{\sigma N}$ through the requirement that there is a cancellation between nucleon-exchange and σ-meson-exchange contributions to zero-four-momentum-transfer pion-nucleon scattering. We impose that relationship, as developed in Sec. III, on all our numerical results.

Results are presented for a variety of values of $g_{\sigma\pi}$ corresponding to σ-meson widths of 100 MeV to 2000 MeV. Particular attention is paid to the 600–700-MeV range of widths which correspond to a soft-pion-dynamics condition proven by Weinberg[6] on the assumption of good asymptotic behavior of tree graphs. This is the same condition that leads to $M_\sigma = M_\rho$ and $M_{A_1} = \sqrt{2}\, M_\rho$, in good agreement with the experimental masses.

The expected large value of $g_{\sigma\pi}$ implies that one cannot neglect higher-order σ-meson-exchange graphs in which the σ meson converts to two pions any number of times. When the two pions are reabsorbed on a nucleon line, vertex radiative corrections are produced which alter both the range and sign of the interaction. The contribution of such graphs is discussed in Sec. II, and the relevant calculations are described in Sec. IV. If the

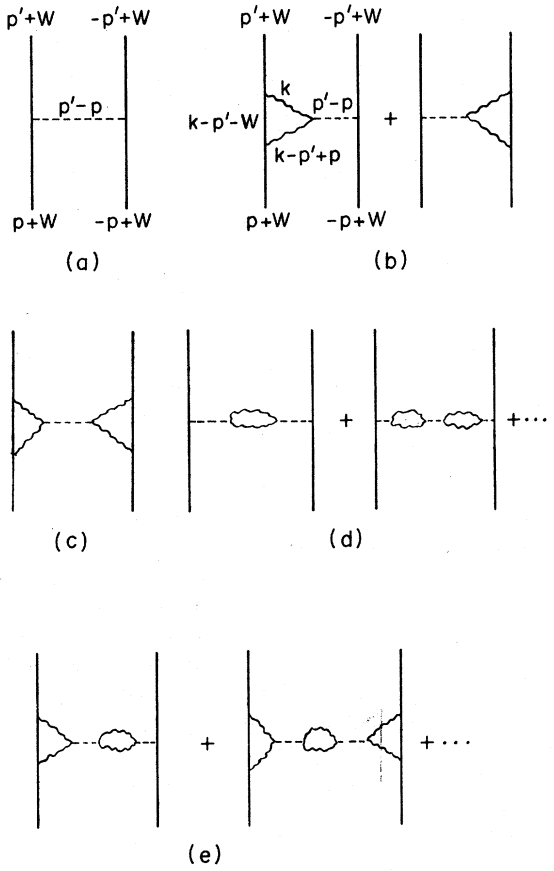

FIG. 1. Nucleon-nucleon scattering diagrams of σ-exchange type. Nucleons are represented by —, pions by ~~, and σ mesons by ----. Momenta in (a) and (b) correspond to Eqs. (15) and (29), respectively.

pions reconvert to a σ meson, bubble diagrams are formed which, summed to all orders, are responsible for the physical mass and width of the σ meson. Their effect is thus treated in Sec. II as a distribution of exchanged-σ-meson masses. All of these effects increase the range of the σ-exchange

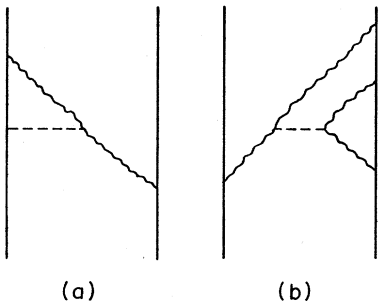

FIG. 2. Nucleon-nucleon scattering one-pion-exchange diagrams with σ-meson radiative corrections to a three-point pion-nucleon vertex. Particles are represented as in Fig. 1.

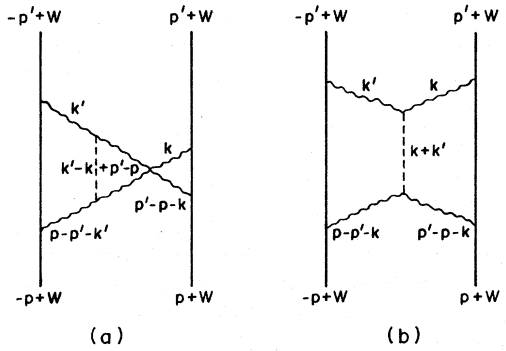

FIG. 3. Nucleon-nucleon scattering two-pion-exchange diagrams with σ-meson corrections to a four-point pion-nucleon scattering vertex. Particles are represented as in Fig. 1. Momenta correspond to Eq. (40).

potential. The opposite sign of the single-pion-pair-vertex correction from the no-pion-pair- and two-pion-pair-vertex terms leads to strong cancellation.

In Sec. V the resultant potentials are presented for various assumed σ-meson widths. Their effect on the total predicted potential is discussed and compared with phenomenological potentials.

II. THE σ-MESON-EXCHANGE CONTRIBUTIONS

The various Feynman diagrams contributing to the single-σ-exchange potential are shown in Figs. 1, 2, and 3. The graphs of these figures differ in having, respectively, one-σ-meson and one- and two-pion simple intermediate t-channel states. The simplest single-σ-meson exchange is that of Fig. 1(a). When the σ meson decays into two pions which are absorbed on one nucleon line, the two diagrams of Fig. 1(b) result. If each meson is absorbed on a different nucleon line diagrams like Fig. 2(a) result. Figure 1(c) is the result of the σ meson decaying into two pions at each end, each pair of pions being absorbed on one nucleon line. In Figs. 3(a) and 3(b) the σ meson decays at both ends but each pair of pions splits to be absorbed on the pair of nucleon lines. Figure 2(b) represents diagrams in which three of the four pions from doubled-ended σ decay go to one nucleon and the fourth meson to the other nucleon. Figure 1(d) represents pion-bubble inserts on the simple σ exchange, while Fig. 1(e) represents bubble inserts on the single- and double-ended σ decay diagrams.

Figure 1 represents direct σ exchange [(a)], modified by vertex corrections (b) and (c) and propagator corrections (d) and (e). The contributions of (a), (b), and (c) to the Bethe-Salpeter-equation kernel and hence to the potential are calculated directly using the techniques of Ref. 1.

The effect of the sum of all bubble inserts of the type of Figs. 1(d) and 1(e) is to change the propagator of the σ meson from that of a stable particle to that of a decaying particle of peak mass M_σ and width Γ_σ. Spectral representations of potentials such as discussed in Ref. 7 allow us to represent that change in the propagator by replacing a δ function by the actual mass distribution of the σ resonance. That spectral function is approximated here by an S-state Breit-Wigner resonance distribution of appropriate mass and width.

The propagator modification to Fig. 1(a), i.e., Fig. 1(d), is most important and hence is calculated in this paper. Figure 1(a) represents a potential of range M_σ^{-1} (we use $\hbar = c = 1$ throughout the paper) while the large width of the σ meson considerably increases the potential range. The replacement of the δ function by a Breit-Wigner distribution in the spectral representation of Fig. 1(a) then produces the effect of the sum of Fig. 1(a) and all the diagrams in Fig. 1(d). The same replacement in the spectral representation of the contribution of Figs. 1(b) and 1(c) would have the effect of summing all the bubble inserts represented by Fig. 1(e). However, the range of the potential from Figs. 1(b) and 1(c) is already extended by the vertex correction to $\frac{1}{2}\mu^{-1}$; i.e., the spectral distribution is nonzero for a spectral mass $M_s \geq 2\mu$, where μ is the pion mass. The Breit-Wigner spreading would cause a folding of a narrow distribution on a broad distribution, leaving the spectral function little altered. We do not compute that small correction here.

Figures 2(a) and 2(b) are actually vertex corrections to one-pion exchange. They are small because of the single pseudoscalar vertex on one nucleon line which introduces a factor of $\mu(2M)^{-1}$ where M is the nucleon mass. In any case their dominant effect is included in the pion-nucleon coupling-constant renormalization. The calculation of the small remainder is not included in this paper.

Figure 3 represents interesting graphs whose Feynman amplitudes will be displayed in integral form for preliminary discussion in this paper. One cannot cut them in the t channel by crossing only the σ-meson line as in Fig. 1; hence they do not represent a single-σ-meson exchange with radiative corrections. Also, as a t-channel cut through a single-pion line cannot be made, they are not pion-nucleon vertex corrections such as in Fig. 2. A t-channel cut can, however, be made through two pion lines so that these diagrams would be included if the full T matrix for pion-nucleon scattering were used in place of the four pion-nucleon vertices and intermediate nucleon propagators. This would also include the diagrams of Fig. 4 which have two σ mesons each.

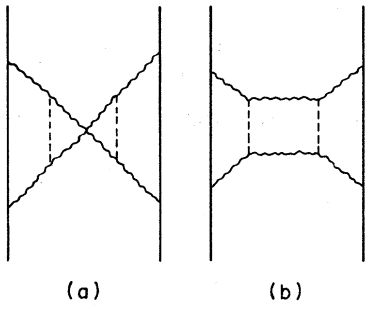

FIG. 4. Nucleon-nucleon scattering two-pion-exchange diagrams with σ-meson corrections to both four-point pion-nucleon scattering vertices. Particles are represented as in Fig. 1.

These corrections are discussed in Sec. VII of Ref. 1 where it is suggested that the sum of all such corrections may best be approximated by including in intermediate states the baryon resonances to which they give rise in the pion-nucleon system. In particular it has been suggested that the σ-nucleon channel gives rise to the "Roper-resonance" P_{11} isobar.[8] This will give rise to P_{11} resonance amplitude differing from a simple Breit-Wigner, and should be included in the NN process as a correction to the treatment of the isobar as a stable particle in intermediate states.

Numerical results of the contribution of Fig. 3 are left for discussion in a future paper in the more relevant context of the consequences of Sec. VII of Ref. 1. However, in Sec. IV, we display the Feynman integrals for Fig. 3, because of their relation to two-pion-exchange and σ-meson-exchange integrals already computed. It can be seen that they will be smaller than the related amplitude of Fig. 1(c). The latter is computed in this paper and is already the smallest of the computed contributions.

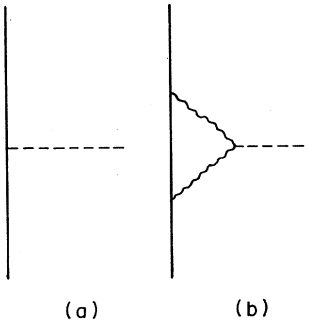

FIG. 5. Contributions to the σ-meson–nucleon three-point function. Figure 5(b) renormalizes Fig. 5(a) in the series of diagrams consistently considered in this paper. Particles are represented as in Fig. 1.

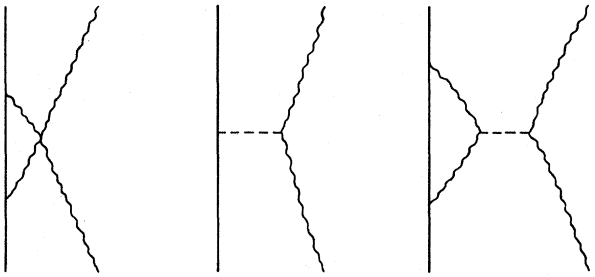

FIG. 6. Pion-nucleon scattering diagrams with σ-exchange corrections. Particles are represented as in Fig. 1.

III. THE σ-MESON COUPLING CONSTANTS AND πN SCATTERING

The numerical values of contributions of Figs. 1, 2, and 3 to the nucleon-nucleon potential are determined by the well-known pion-nucleon coupling constant $g_{\pi N}$ ($g_{\pi N}^2/4\pi \approx 15$) and by the lesser-known $g_{\sigma N}$ and $g_{\sigma\pi}$. We reserve this notation for the coupling strength appropriate to our restricted set of diagrams. Hence $g_{\pi N}$ and $g_{\sigma\pi}$ include all vertex renormalizations, but $g_{\sigma N}$ of Fig. 5(a) is to be modified by Fig. 5(b). The width of the σ meson (to two-pion decay) is known to be large so that[5] $g_{\sigma\pi} \gtrsim 0.3 g_{\pi N}$. Our predictions are qualitatively the same for all such $g_{\sigma\pi}$ providing that $g_{\sigma N}$ is chosen for each $g_{\sigma\pi}$ to correspond to a general current-algebra rule.[9] A somewhat more special current-algebra result[6] is used to determine a particular $g_{\sigma\pi}$ and hence a unique prediction.

In Ref. 9 Weinberg demonstrates, using only the current commutation relations and partial conservation of axial-vector current (PCAC), that the even-isospin-exchange term vanishes for pion-nucleon scattering in the zero-four-momentum-transfer limit. This requires that the large zero-isospin-exchange term due to the nucleon-pole graph [Fig. 6(a)] be canceled by other terms at zero four-momentum transfer. In any specific chiral-invariant model in which only the nucleon-pole and σ-exchange graphs contribute to πN scattering this means that Fig. 6(b) must cancel Fig. 6(a) in that limit, which imposes a condition on the (properly renormalized) product of $g_{\sigma N}$ and $g_{\sigma\pi}$. The calculation of Figs. 6(a) and 6(b) in the zero-four-momentum limit is simple and leads to the simple cancellation condition

$$g_{\sigma N}^R g_{\sigma\pi}^R = \tfrac{1}{2} M^{-1}(M_\sigma^2 - \mu^2)(g_{\pi N}^R)^2 . \tag{1}$$

The couplings $g_{\sigma\pi}$ and $g_{\pi N}$ are renormalized in that they are given by the σ-meson decay width and the known physical $\pi N\bar{N}$ coupling, respectively. As no radiative corrections are in the included class of diagrams, we use

$$g_{\sigma\pi}^R = g_{\sigma\pi} \quad \text{and} \quad g_{\pi N}^R = g_{\pi N}, \tag{2}$$

where $g_{\sigma N}$ is obtained from the σ-meson decay rate (width) and $g_{\pi N}$ from the physical πN vertex strength (i.e., $g^2/4\pi \approx 15$). The $\sigma N\bar{N}$ coupling is explicitly labeled by a superscript R for renormalization to be consistent with the fact that in our Lagrangian-type theory we have included Figs. 1(a)–1(c) as separate contributions. Hence $g_{\sigma N}^R$ is determined by the sum of Figs. 6(b) and 6(c) at zero four-momentum transfer, where each of those figures have $\sigma N\bar{N}$ vertices with the $g_{\sigma N}$ coupling only. A simple calculation shows that Fig. 6(b) with $g_{\sigma N}^R$ would give the result of Figs. 6(b) and 6(c) with $g_{\sigma N}$ if

$$g_{\sigma N}^R = g_{\sigma N} - 6 g_{\pi N}^2 g_{\sigma\pi}(4\pi)^{-2} g(M), \tag{3}$$

where

$$\begin{aligned} g(M) &= \int_0^1 y\,dy \int_0^1 x^2 dx M(M^2x^2y^2 - \mu^2 xy + \mu^2)^{-1} \\ &= -M^{-1} + M^{-3}(M^2 - \mu^2)\ln(M/\mu) \\ &\quad + \mu M^{-3}(4M^2 - \mu^2)^{-1/2}(3M^2 - \mu^2)\cos^{-1}(\tfrac{1}{2}\mu/M) . \end{aligned} \tag{4}$$

Equation (3) is used to obtain $g_{\sigma N}$ for use in nucleon-nucleon graphs, given $g_{\sigma N}^R$ obeying Eqs. (1) and (2).

The explicit "σ-model" chiral-invariant Lagrangian due to Gell-Mann and Lévy[10] combines the σ with the pseudoscalar-meson–nucleon interaction in the form

$$\mathcal{L}_{\mathrm{GL}}(\text{meson-nucleon}) = g_{\pi N}^R \bar{N}(\sigma + i\vec{\tau}\cdot\vec{\pi}\gamma_5)N . \tag{5}$$

Hence

$$g_{\sigma N} = g_{\pi N} \tag{6a}$$

and their Lagrangian contains a $\sigma\vec{\pi}\cdot\vec{\pi}$ term such that

$$g_{\sigma\pi} = \tfrac{1}{2} M^{-1}(M_\sigma^2 - \mu^2) g_{\pi N} . \tag{6b}$$

Equation (1) is satisfied by Eqs. (6a) and (6b), a necessary consequence of chiral algebra, PCAC, and the absence of other particles from the σ model.

We note here for later numerical comparisons that axial-vector-current renormalization in current algebra requires (see footnote 8 of Ref. 11) the value of $g_{\sigma\pi}$ given by Eq. (6b) be multiplied by g_V/g_A (the ratio of the vector to the axial-vector weak coupling constants). Hence $g_{\sigma N}$ must be multiplied by g_A/g_V to maintain the cancellation leading to the Adler self-consistency PCAC condition[12] as needed in a strict Lagrangian σ model. Both of

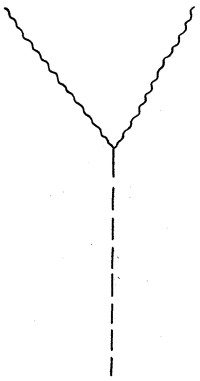

FIG. 7. Diagram for σ-meson decay. Particles are represented as in Fig. 1.

these renormalizations are given by the rule: Multiply by g_V/g_A for each soft-pion line and by g_A/g_V for each σ-meson line at a vertex. The result is

$$g^R_{\sigma N} = (g_A/g_V) g^R_{\pi N} \tag{7a}$$

and

$$g^R_{\sigma\pi} = \tfrac{1}{2} M^{-1}(M_\sigma{}^2 - \mu^2)(g_V/g_A) g^R_{\pi N} \tag{7b}$$

still satisfying Eq. (1).

However, a chiral-invariant system[6] that contains the ρ and A_1 mesons and the $P_{33}(\Delta)$ and P_{11} nucleon isobars as well as the π and σ mesons also satisfies Eq. (1) while differing from Eqs. (7a) and (7b). This system was proposed by Weinberg and is a minimal system satisfying physical asymptotic conditions of the sum of tree graphs. Equation (5) is replaced by

$$\mathfrak{L}_W(\text{meson-nucleon}) = g_{\sigma N}\bar{N}(v_4 + i\vec{\tau}\cdot\vec{\mathbf{v}}\gamma_5)N, \tag{8}$$

where

$$v_4 = \sigma \quad \text{and} \quad \vec{\mathbf{v}} = \sin\psi\,\vec{\pi} + \cos\psi\,\vec{\mathbf{A}}_1 \tag{9}$$

with $\psi = 45°$ by Weinberg's asymptotic condition.

It follows that

$$g_{\pi N} = (2)^{-1/2} g_{\sigma N}. \tag{10a}$$

Equation (10a) is to be used to determine $g^R_{\sigma N}$ in terms of the well-known $g^R_{\pi N}$. The A_1 meson does not affect the πN scattering [Figs. 6(a)–6(c)] because its negative G parity prevents it from coupling to the two external pion lines. It will be of small importance to nucleon forces because of its high mass and small width.

Reference 6 shows that

$$g_{\sigma\pi} = \tfrac{1}{2} M^{-1}(M_\sigma{}^2 - \mu^2) g_{\pi N} \sin\psi, \tag{10b}$$

with

$$\sin\psi = (2)^{-1/2}.$$

Taking into account axial-vector-current renormalization we get

$$g^R_{\sigma N} = \sqrt{2}(g_A/g_V) g^R_{\pi N} \tag{11a}$$

and

$$g^R_{\sigma\pi} = (2)^{-3/2}(g_V/g_A) M^{-1}(M_\sigma{}^2 - \mu^2) g^R_{\pi N}, \tag{11b}$$

which again satisfies Eq. (1), but leads to a σ-meson decay width one half as large as Eq. (7b).

P_{11} and P_{33} pole diagrams in πN scattering cancel in the soft-pion limit, as given by the transformation matrix elements of Ref. 6. The independent cancellation of the σ-meson exchange with the nucleon-pole diagram remains in this soft-pion theory.

We shall assume Eq. (1) to hold in all our numerical calculations. However, it is possible that some acceptable representation of chiral algebra and PCAC depends on a πN scattering-amplitude cancellation in which the nucleon-pole and σ-meson-exchange diagrams do not cancel between themselves. In such a case very different results would be possible.

We conclude this section with the relationship between $g^R_{\sigma\pi}$ and the σ decay width. A straightforward calculation of the rate from Fig. 7 gives

$$\Gamma_\sigma = 3(8\pi M_\sigma)^{-1}[1 - (2\mu/M_\sigma)^2]^{1/2}(g^R_{\sigma\pi})^2. \tag{12}$$

We note that the use of Weinberg's result, Eq. (11b), gives a numerical value of $\Gamma_\sigma = 610$ MeV if $m_\sigma = m_\rho$ and g_A/g_V is determined by the Goldberger-Treiman relation

$$g_A/g_V \approx \tfrac{1}{2} M^{-1} g_{\pi N} F_\pi \approx 1.37, \tag{13}$$

with $F_\pi = 190$ MeV corresponding to a ρ-meson decay width $\Gamma_\rho = 118$ MeV. If the value $\Gamma_\rho = 133$ MeV is used, then $F_\pi = 180$ MeV and $g_A/g_V \approx 1.30$, predicting $\Gamma_\sigma = 680$ MeV. We note that the latest experimental analysis of the σ meson is in good agreement with Weinberg's theory.[5] The original σ model predicts twice the Weinberg width, while some experimental analyses have indicated widths as low as 200–300 MeV.

Using an experimental value for $g_A/g_V \approx 1.18$, Eqs. (11b) and (12) yield $\Gamma_\sigma = 850$ MeV.

IV. CALCULATION OF σ-MESON-EXCHANGE POTENTIAL

In this section we present the integrals for the potentials defined by Fig. 1(a) and the corrections indicated by Fig. 1(d), by Fig. 1(b), and by Fig. 1(c). Although the method is described in Ref. 1, we shall for clarity review the essential steps for Fig. 1(a).

Direct σ-meson exchange: For the usual scalar-meson–nucleon Hamiltonian

$$H_\sigma = g_{\sigma N}\bar{N}\sigma N, \tag{14}$$

the relativistic second-order amplitude produces the kernel for the Bethe-Salpeter amplitude

$$K_\sigma^{(2)} = -(2\pi)^{-3} g_{\sigma N}{}^2 1^{(1)} 1^{(2)} \omega^{-2}, \tag{15}$$

where $1^{(i)}$ is the identity operator on the ith nucleon and

$$\omega^2 = \Delta^2 + M_\sigma{}^2, \quad \vec{\Delta} = \vec{p}' - \vec{p}, \tag{16}$$

where $\vec{p}$ ($\vec{p}'$) is the initial (final) relative momentum of the two nucleons.

To obtain the appropriate momentum-space potential, the matrix element of the kernel is taken between the initial- and final-state (positive-energy) spinors and a kinematic factor is required to compensate for the change from relativistic to nonrelativistic unitarity.[1]

$$\begin{aligned}\chi_{s_1'}^\dagger \chi_{s_2'}^\dagger V^\sigma(\vec{\Delta}, \vec{Q}) \chi_{s_1} \chi_{s_2} &= (M/E')^{1/2} \bar{u}_1(\vec{p}', s_1') \bar{u}_2(-\vec{p}', s_2') \\ &\times K_\sigma^{(2)} u_1(\vec{p}, s_1) u_2(-\vec{p}, s_2) (M/E)^{1/2},\end{aligned} \tag{17}$$

with

$$\vec{Q} = \vec{p}' + \vec{p}, \quad E = (p^2 + M^2)^{1/2}, \quad E' = (p'^2 + M^2)^{1/2}.$$

We have

$$u^{(i)}(p, s_i) = (2M)^{-1/2}(E+M)^{1/2} \begin{pmatrix} \chi_{s_i} \\ -\dfrac{\vec{\sigma}^{(i)} \cdot \vec{p}}{E+M} \chi_{s_i} \end{pmatrix} \tag{18}$$

and $\bar{u}^i(p, s_i)$ is its Pauli adjoint, where χ_{si} is the Pauli spinor for the ith nucleon.

Expanding to first order in Q, but making no approximation in Δ, Eqs. (17) and (18) lead to

$$V^\sigma(\vec{\Delta}, \vec{Q}) = V_c(\Delta) + \tfrac{1}{2} i \vec{\Sigma} \cdot (\vec{\Delta} \times \vec{Q}) V_{so}(\Delta), \tag{19}$$

with

$$\vec{\Sigma} = \tfrac{1}{2}(\vec{\sigma}_1 + \vec{\sigma}_2)$$

and

$$V_c^\sigma(\Delta) = -(2\pi)^{-3} g_{\sigma N}{}^2 M^{-1} D \omega^{-2}, \tag{20}$$

$$V_{so}^\sigma(\Delta) = 4(2\pi)^{-3} g_{\sigma N}{}^2 M^{-1} (D - M) \omega^{-2}, \tag{21}$$

with

$$\omega^2 = \Delta^2 + M_\sigma{}^2 \quad \text{and} \quad D^2 = M^2 + \tfrac{1}{4}\Delta^2.$$

The configuration-space potential is then obtained by a Fourier transform of $V^\sigma(\vec{\Delta}, \vec{Q})$

$$V^\sigma(\vec{r}) = V_c^\sigma(r) + \vec{L} \cdot \vec{\Sigma} V_{so}^\sigma(r), \tag{22}$$

with

$$\begin{aligned} V_c^\sigma(r) &= \int d^3\Delta\, e^{-i\vec{\Delta}\cdot\vec{r}} V_c^\sigma(\Delta) \\ &= g_{\sigma N}{}^2 (1-\alpha^2)^{-1/2} (4\pi r)^{-1} e^{-M\sigma r} - \tfrac{1}{2}\pi^{-2} g_{\sigma N}{}^2 r^{-1} \int_1^\infty t\, dt (t^2-1)^{1/2} (t^2-\alpha^2)^{-1} e^{-2Mrt} \end{aligned} \tag{23}$$

and

$$\begin{aligned} V_{so}^\sigma(r) &= r^{-1} \frac{d}{dr} \int d^3\Delta\, e^{-i\vec{\Delta}\cdot\vec{r}} V_{so}^\sigma(\Delta) \\ &= \pi^{-1} M_\sigma{}^{-2} g_{\sigma N}{}^2 [1 - (1-\alpha)^{1/2}](r^{-3} + M_\sigma r^{-2}) e^{-M_\sigma r} + \tfrac{1}{2}\pi^{-2} g_{\sigma N}{}^2 M^{-1} r^{-2} \int_1^\infty dt \left(2 + \frac{1}{Mrt}\right)(t^2-1)^{1/2}(t^2-\alpha^2)^{-1} e^{-2Mrt}, \end{aligned} \tag{24}$$

with

$$\alpha = M_\sigma/(2M).$$

The integrals in Eqs. (23) and (24) [which come from the contour integration over the cuts of $V^\sigma(\vec{\Delta}, \vec{Q})$] are strongly damped by the e^{-2Mrt} factors. For $r \geq \frac{1}{2}\mu^{-1}$ they are less than 0.1% of the first terms which arise from the pole of $V^\sigma(\vec{\Delta}, \vec{Q})$. We shall neglect the cut contribution in considering the effect of Fig. 1(d) contributions.

Bubble-diagram inserts: The bubble diagrams to all orders such as those in Fig. 1(d) have the effect of shifting the σ-meson mass to its physical value and also of producing a decay width. Analytically it moves the pole off the real energy axis onto the second sheet, and in the pole approximation one obtains the Breit-Wigner formula for the spectral distribution on the real axis. Taking into account the elastic threshold behavior for an S-wave π-π system in addition to the resonance pole, but no other singularities, one obtains the spectral distribution

$$\rho(m^2) = N m^{-2}(m^2 - 4\mu^2)[(m^2 - M_\sigma{}^2)^2 + M_\sigma{}^2 \Gamma_\sigma{}^2]^{-1}, \tag{25}$$

with normalization

$$N^{-1} = \int_{4\mu^2}^\infty \frac{m^{-2}(m^2 - 4\mu^2) dm^2}{(m^2 - M_\sigma{}^2)^2 + M_\sigma{}^2 \Gamma_\sigma{}^2}$$

and m being the mass variable of the "spread" σ meson.

In the approximation that the mass spread is the only important consequence of the sum of bubble diagrams the appropriate potential due to Figs. 1(a) and 1(d) is obtained from

$$V_\lambda^{\sigma\Gamma}(r)=\int_{4\mu^2}^{4M^2} dm^2\rho(m^2)V_\lambda^\sigma(m,r), \tag{26}$$

where $V_c^\sigma(m,r)$ and $V_{so}^\sigma(m,r)$ are obtained from Eqs. (23) and (24) by substituting m for M_σ. Dropping the inconsequential integral contributions we have

$$V_c^\sigma(m,r)=-g_{\sigma N}^2(8\pi Mr)^{-1}(4M^2-m^2)^{1/2}e^{-mr}$$

and (27)

$$V_{so}^\sigma(m,r)=-g_{\sigma N}^2(2\pi Mr)^{-1}(mr)^{-2}(1+mr)\times[2M-(4M^2-m^2)^{1/2}]e^{-mr}.$$

The upper limit on the integral of Eq. (26) is put at $4M^2$ because $\rho(m)$ is small in this region and beyond. At $m^2=4M^2$ the $(4M^2-m^2)^{1/2}$ factors cause both the pole and cut contributions to Eqs. (23) and (24) to have canceling imaginary parts. The real part of the pole term like the cut term is small for $m^2\approx 4M^2$. Hence it is consistent with the reality of the sum and the neglect of the cut term to stop the integration at that point.

σ-meson and two-pion exchange: The two graphs of Fig. 1(b) represent the case of a direct σ-nucleon vertex on one nucleon, with the decay of the σ meson and absorption of both decay pions on the other nucleon. The relativistic perturbation theory for these graphs produces the amplitude

$$K_{\sigma\pi}^{(4)}=-6i(2\pi)^{-3}g_{\pi N}^2 g_{\sigma\pi}g_{\sigma N}[(p'-p)^2-M_\sigma^2]^{-1}(I_1+I_2), \tag{28}$$

with

$$I_1=(2\pi)^{-4}\int d^4k\,\gamma_5^{(1)}\frac{\gamma^{(1)}\cdot(W+p'-k)+M}{(k-p'-W)^2-M^2}\times\gamma_5^{(1)}\frac{(k^2-\mu^2)^{-1}}{(k-p'+p)^2-\mu^2} \tag{29}$$

and

$$I_2=I_1(p\to -p,\ p'\to -p',\ \gamma^{(1)}\to\gamma^{(2)}),$$

where the notation is that the four-momenta of the two nucleons are $W+p$ and $W-p$, so that $p^0=p'^0=0$. The energy is expressed by $2W$.

We expand to linear terms in $\vec{Q}$ and use the Pauli representation of the spinors to that order as follows:

$$1^{(1)}1^{(2)}\to\phi^2(\Delta^2)-4\Delta^{-2}\phi(\Delta^2)[\phi(\Delta^2)-1]\tfrac{1}{2}i\vec{\Sigma}\cdot(\vec{\Delta}\times\vec{Q}), \tag{30}$$

$$\gamma_0^{(1)}1^{(2)}+\gamma_0^{(2)}1^{(1)}\to 2\phi(\Delta^2)+4\Delta^{-2}[\phi(\Delta^2)-1]^2\tfrac{1}{2}i\vec{\Sigma}\cdot(\vec{\Delta}\times\vec{Q}),$$

with

$$\phi(z)=[1+(2M)^{-2}z]^{1/2}.$$

We get

$$M(EE')^{-1/2}(I_1+I_2)_c=-2Mi(4\pi)^{-2}\int_0^1 dy\int_0^1 x\,dx\,D^{-1}\{xy\phi(\Delta^2)+(xy-1)[1-\phi(\Delta^2)]\},$$
$$M(EE')^{-1/2}(I_1+I_2)_{so}=4Mi(4\pi)^{-2}\int_0^1 dy\int_0^1 x\,dx\,D^{-1}\{2xy[\phi(\Delta^2)-1]+(xy-1)\phi^{-1}(\Delta^2)[1-\phi(\Delta^2)]^3\}, \tag{31}$$

with

$$D=M^2x^2y^2+\mu^2(1-xy)+\Delta^2[x(1-x)(1-y)+\tfrac{1}{4}xy(1-xy)].$$

It is found that putting the external legs on the mass shell, i.e., $\vec{p}^2=\vec{p}'^2=W^2-M^2$, results in a negligible alteration of the above results. This is equivalent to dropping the second term in each integrand (i.e., those proportional to $xy-1$) and the term $\frac{1}{4}xy(1-xy)$ in D.[13]

Defining the configuration-space potential as in Eqs. (23) and (24), we have

$$V_c^{\sigma\pi}(r)=-i\lambda_{\sigma\pi}r^{-1}\int_0^1\frac{y\,dy}{1-y}\int_0^1\frac{x\,dx}{1-x}\int_{-\infty}^{\infty}\frac{\Delta e^{ir\Delta}\phi(\Delta^2)}{(\Delta^2+M_\sigma^2)(\Delta^2+\tau_{xy})}d\Delta \tag{32}$$

and

$$V_{so}^{\sigma\pi}(r)=4i\lambda_{\sigma\pi}r^{-1}\frac{d}{dr}\left(r^{-1}\int_0^1\frac{y\,dy}{1-y}\int_0^1\frac{x\,dx}{1-x}\int_{-\infty}^{\infty}\frac{\Delta^{-1}e^{ir\Delta}[\phi(\Delta^2)-1]}{(\Delta^2+M_\sigma^2)(\Delta^2+\tau_{xy})}d\Delta\right), \tag{33}$$

with

$$\lambda_{\sigma\pi}=3(2\pi)^{-4}g_{\sigma\pi}g_{\sigma N}g_{\pi N}^2M$$

and (34)

$$\tau_{xy}=x^{-1}(1-x)^{-1}(1-y)^{-1}[M^2x^2y^2+\mu^2(1-xy)].$$

In performing the integral over Δ by contour integration in the upper half plane, one obtains contributions from the poles at iM_σ and $i\sqrt{\tau}$ and from the cut with branch point at $2iM$. We have verified that the cut contribution is less than 1%. As in the case of direct σ-meson exchange, the cut term can be ignored together with contributions to the integral from the term proportional to $e^{-r\sqrt{\tau}}$ for which $\tau > 4M^2$. Hence

$$V_c^{\sigma\pi}(r) \approx -\lambda_{\sigma\pi} r^{-1} \int_0^1 \frac{y\,dy}{1-y} \int_0^1 \frac{x\,dx}{1-x} \frac{\phi(-M_\sigma^2)e^{-M_\sigma r} - \bar{\phi}(-\tau)e^{-r\sqrt{\tau}}}{M_\sigma^2 - \tau_{xy}} \tag{35}$$

and

$$V_{so}^{\sigma\pi}(r) \approx -4\lambda_{\sigma\pi} r^{-3} \int_0^1 \frac{y\,dy}{1-y} \int_0^1 \frac{x\,dx}{1-x} (M_\sigma^2 - \tau_{xy})^{-1}$$

$$\times \{\tau(1+r\sqrt{\tau})[1-\bar{\phi}(-\tau)]e^{-r\sqrt{\tau}} - M_\sigma^{-2}(1+M_\sigma r)[1-\phi(-M_\sigma^2)]e^{-M_\sigma r}\} \tag{36}$$

in which

$$\bar{\phi}(\tau) = \phi(\tau)\theta(4M^2 - \tau).$$

The coefficients of $e^{-M_\sigma r}$ in Eqs. (35) and (36) can be reduced to single integrals using $R(M_\sigma^2)$ where

$$R(\beta) \equiv \int_0^1 y\,dy \int_0^1 x^2 dx [M^2x^2y^2 - \mu^2(1-xy) - x(1-x)(1-y)\beta]^{-1}$$

$$= \frac{1}{2}\int_0^1 c^{-2} y\,dy \{-b \ln[(1-y)\mu^2 + M^2y^2] + (b^2 - 2c) f(y)\}, \tag{37}$$

with

$$b = -y\mu^2 - (1-y)\beta, \quad c = M^2y^2 + (1-y)\beta$$

and given $q = b^2 - 4\mu^2 c$,

$$f(z) = \begin{cases} q^{-1/2} \ln(2\mu^2 + b + q^{1/2})(2\mu^2 + b - q^{1/2})^{-1} & q > 0 \\ 2(-q)^{-1/2} \tan^{-1}(-q)^{-1/2}(2\mu^2 + b)^{-1} & q < 0. \end{cases}$$

σ-meson and double two-pion exchange: The graph of Fig. 1(c) represents the case in which the exchanged σ meson decays at both ends and each pair of decay pions is absorbed on a single nucleon line. The corresponding Feynman integral requires integration over two loops. However, the momentum integrals factorize into I_1 and I_2 of Eq. (29) because of the separation of the loops by the σ-meson propagator whose 4-momentum is the fixed momentum transfer. Making the same expansions and numerical approximations as in Eqs. (30) to (36) we obtain

$$V_c^{\sigma\pi\pi}(r) = -\lambda_{\sigma\pi\pi} r^{-1} \left\{ \phi(-M_\sigma^2)[R(M_\sigma^2)]^2 e^{-M_\sigma r} + 2\int_0^1 \frac{y\,dy}{1-y} \int_0^1 \frac{x\,dx}{1-x} \frac{\bar{\phi}(-\tau)e^{-r\sqrt{\tau}}}{M_\sigma^2 - \tau_{xy}} R(\tau_{xy}) \right\} \tag{38}$$

and

$$V_{so}^{\sigma\pi\pi}(r) = -4\lambda_{\sigma\pi\pi} r^{-3} \left\{ [1-\phi(-M_\sigma^2)] M_\sigma^{-2}(1+M_\sigma r)[R(M_\sigma^2)]^2 e^{-M_\sigma r} \right.$$

$$\left. + 2\int_0^1 \frac{y\,dy}{1-y} \int_0^1 \frac{x\,dx}{1-x} \frac{1-\bar{\phi}(-\tau)}{M_\sigma^2 - \tau_{xy}} \tau_{xy}^{-1/2}(1 + r\tau_{xy}^{1/2}) R(\tau_{xy}) e^{-r\sqrt{\tau}} \right\}, \tag{39}$$

with

$$\lambda_{\sigma\pi\pi} = 9(2)^{-8}\pi^{-5} g_{\sigma\pi}^2 g_{\pi N}^4 M^2.$$

σ-meson corrections to pion-nucleon scattering vertices: As discussed in Sec. II the diagrams of Fig. 3 are not σ-meson-exchange contributions, but rather σ-meson vertex corrections to pion-nucleon scattering. As such they should be included with the nucleon-isobar intermediate-state corrections to the nucleon-nucleon potential. Their algebraic structure is similar to that of the previous section and we present the form here for future use. The amplitudes are labeled by the figure number.

$$K^{3a,b} \sim (3 \mp \vec{\tau}_1 \cdot \vec{\tau}_2) \int d^4k \int d^4k' \gamma_5^{(1)} [\gamma^{(1)} \cdot (W + p' - k) + M][(k - p' + W)^2 - M^2]^{-1}$$
$$\times \gamma_5^{(1)} \gamma_5^{(2)} [\gamma^{(2)} \cdot (W - p' - k) + M][(k' + p' - W)^2 - M^2]^{-1} \gamma_5^{(2)}$$
$$\times \{(\chi_{a,b}{}^2 - M_\sigma{}^2)(k^2 - \mu^2)(k'^2 - \mu^2)[(k - p' + p)^2 - \mu^2][(k' + p' - p)^2 - \mu^2]\}^{-1}, \quad (40)$$

with $\chi_a = k' - k + p' - p$ and $\chi_b = k' + k$. The mixing of k and k' in χ_a or χ_b prevents the factorization into independent integrals. The presence of $\chi_{a,b}{}^2$ in the denominator will lessen the contribution of Eq. (40) with respect to that of Eqs. (38) and (39) in which $(p' - p)^2 - M_\sigma{}^2$ appears in the denominator. The latter are already small compared to $V^{\sigma\Gamma}$ and $V^{\sigma\pi}$. Note the appearance of an isospin dependence of the type obtained in two-pion exchange.

Bubble inserts on $V^{\sigma\pi}$ and $V^{\sigma\pi\pi}$: To obtain the effect of summing the bubble diagrams of Fig. 1(e), the potentials of Eqs. (35), (36), (38), and (39) need only be inserted into Eq. (26).

V. RESULTS AND CONCLUSIONS

Tables I and II give results for the central and spin-orbit potentials, respectively, of the contributions of V^σ [Eqs. (23) and (24)], $V^{\sigma\Gamma}$ [Eqs. (26) and (27)], $V^{\sigma\pi}$ [Eqs. (35) and (36)], and $V^{\sigma\pi\pi}$ [Eqs. (38) and (39)]. Both $V^{\sigma\pi}$ and $V^{\sigma\pi\pi}$ decrease much more slowly than V^σ with distance, as expected

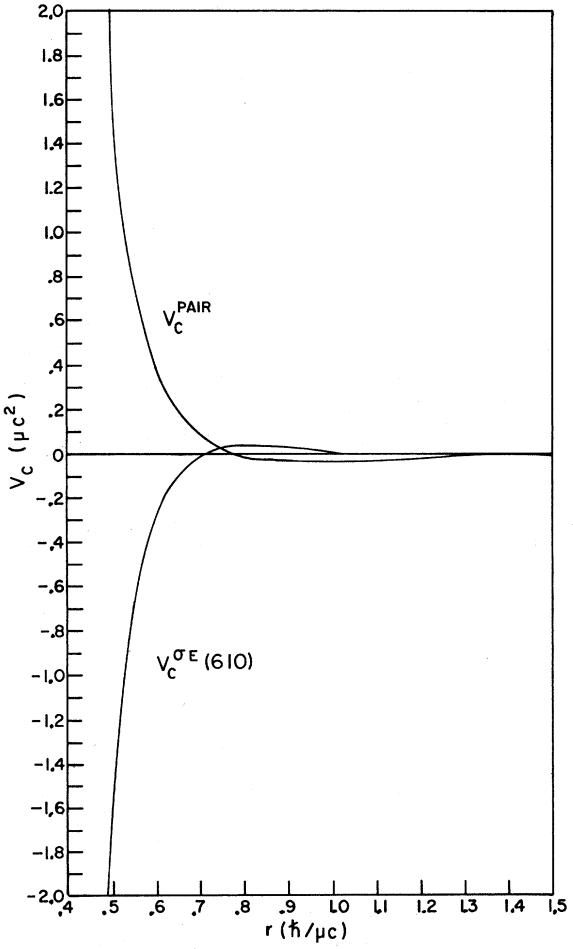

FIG. 8. The σ-exchange central nucleon-nucleon potential for $\Gamma_\sigma = 610$ MeV conpared to the nonrelativistic one- and two-nucleon pair contributions to the central nucleon-nucleon potential (Ref. 15). $M_\sigma = 765$ MeV.

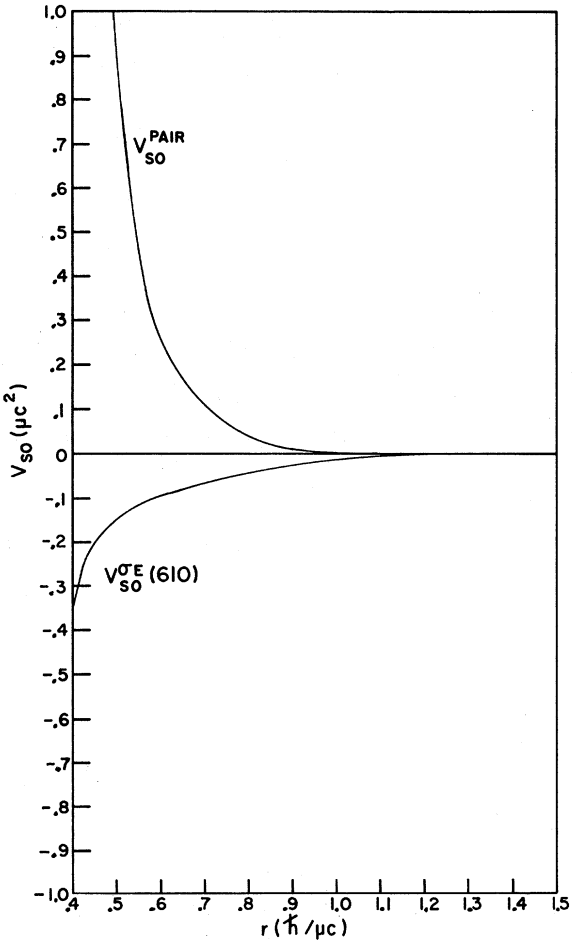

FIG. 9. The σ-exchange spin-orbit nucleon-nucleon potential for $\Gamma_\sigma = 610$ MeV compared to the nonrelativistic two-nucleon-pair contributions to the spin-orbit nucleon-nucleon potential (Ref. 15). $M_\sigma = 765$ MeV.

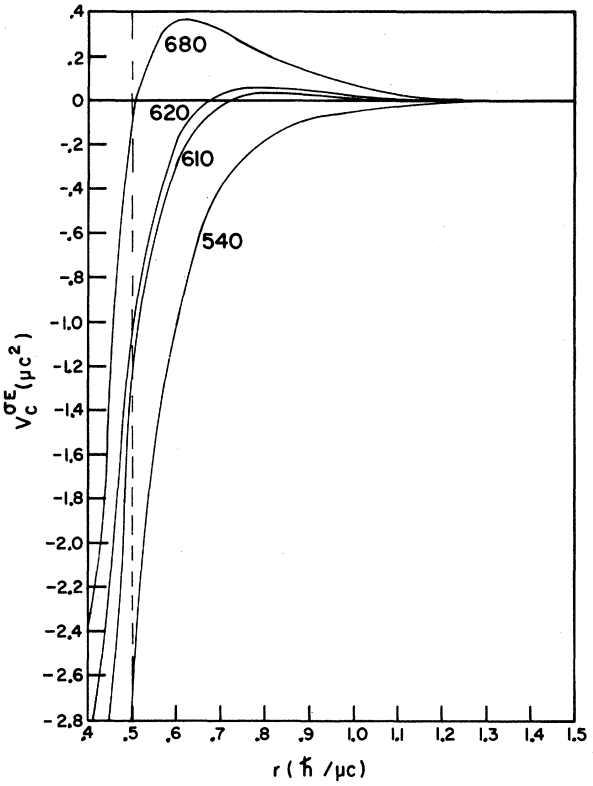

FIG. 10. The σ-exchange central nucleon-nucleon potentials for Γ_σ near the value predicted by Ref. 6. $M_\sigma = 765$ MeV.

due to the two-pion-exchange component of the first pair. However, $V^{\sigma\Gamma}$, which replaces V^σ when bubble diagrams are added, has an r dependence much more like $V^{\sigma\pi}$ than like V^σ, although it still decreases faster than $V^{\sigma\pi}$. The similar r dependence together with opposing signs of $V^{\sigma\pi}$ with respect to $V^{\sigma\Gamma}$ and $V^{\sigma\pi\pi}$ cause extensive cancellation in the sum $V^{\sigma E} = V^{\sigma\Gamma} + V^{\sigma\pi} + V^{\sigma\pi\pi}$. The degree of cancellation depends on the coupling constants. The constraint of Eq. (1) (which implies cancellation among the diagrams of Fig. 6 for zero-four-momentum pion-nucleon scattering) tends to maintain approximate cancellation of $V^{\sigma E}$.

For the numerical results discussed here we have chosen $(4\pi)^{-1} g_{\pi N}^2 = 14.4$ (as in Ref. 1) and maintain the condition of Eq. (1). A choice of the mass and width of the σ meson then determines all the constants through the use of Eqs. (12) and (3). We have chosen $M_\sigma = M_\rho = 765$ MeV which is suggested by several Veneziano[14] and soft-pion models (including Ref. 6) and is in agreement with experiment.[5] We have calculated the potentials using $M_\sigma = 730$ MeV also. Although parts of the potential differ by up to 30% from that calculated with 765 MeV, a small change in σ-meson width will restore the character of the predicted $V^{\sigma E}$, so that

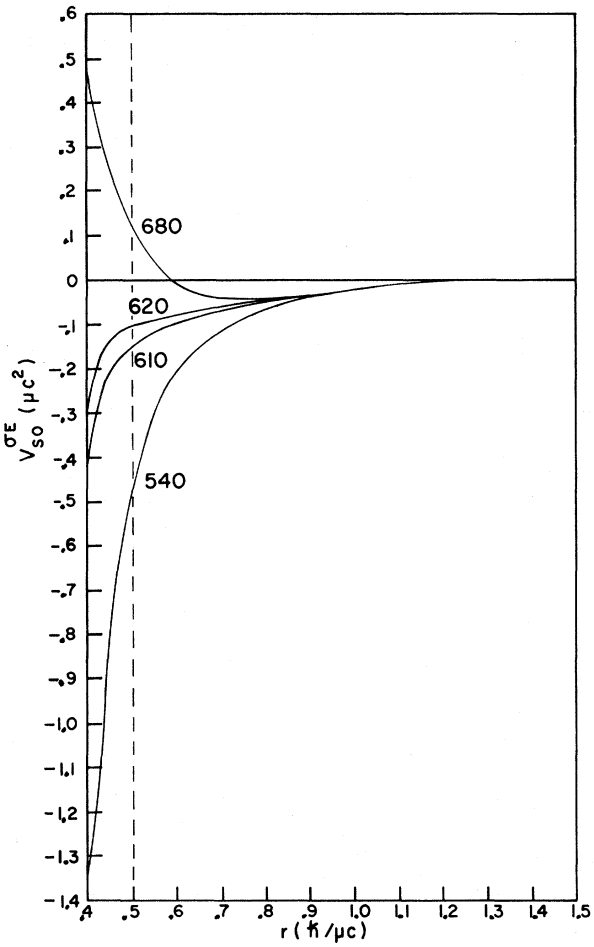

FIG. 11. The σ-exchange spin-orbit nucleon-nucleon potentials for Γ_σ near the value predicted by Ref. 6. $M_\sigma = 765$ MeV.

all of the present conclusions would not change.

Tables I and II correspond to the choice $\Gamma_\sigma = 620$ MeV, which is consistent with the prediction of Ref. 6. It is also the choice for which the cancellation is optimized in the range $r > \frac{1}{2}\mu^{-1}$. The important effect of coupling-constant renormalization according to Eq. (3) should be noted. The coupling constants are given in Tables I and II.

The $\Gamma_\sigma = 610$ MeV results are shown in Figs. 8 and 9. On the same graphs we show the nonrelativistic approximation V^P to the potential arising from the time-ordered two-meson-exchange graphs in which there are nucleon-antinucleon pairs in intermediate states. The central potential is the sum of one and two "pair" terms as given by Klein[15] and incorporated in the perturbation potential of Lomon and Feshbach.[16] The spin-orbit potential shown is that arising from the two "pair" term and given in an appendix of Ref. 15. It is remarkable that for the chosen value of Γ_σ the σ-meson-exchange potential does significantly cancel

TABLE I. σ-meson-exchange contributions to the central potential. $(g^R_{\pi N})^2/4\pi = 14.4$, $(g_{\sigma N})^2/4\pi = 157.5$, $(g^R_{\sigma N})^2/4\pi = 55.4$ [Eq. (3)], and $(g^R_{\sigma\pi})^2/4\pi = 17.43\mu^2$ corresponding to $\Gamma_\sigma = 620$ MeV. Equation (1) is satisfied.

r (μ^{-1})	V_c^σ (μ)	ΔV_c^σ(cut) [a] (μ)	$V_c^{\sigma\Gamma}$ (μ)	$V_c^{\sigma\pi}$ (μ)	$V_c^{\sigma\pi\pi}$ (μ)	$V_c^{\sigma E}$ (μ)
0.40	−40.27	−0.1112	−31.57	34.79	−7.75	−4.538
0.50	−18.59	−0.0172	−15.34	18.77	−4.56	−1.123
0.60	−8.95	−0.0029	−7.94	10.52	−2.75	−0.169
0.70	−4.43	−0.0005	−4.31	6.05	−1.69	0.044
0.80	−2.24	−0.0001	−2.44	3.56	−1.06	0.064
0.90	−1.15	−0.0000	−1.42	2.14	−0.68	0.042
1.00	−0.60	−0.0000	−0.85	1.31	−0.44	0.020
1.10	−0.32	−0.0000	−0.53	0.82	−0.29	0.006
1.20	−0.17	−0.0000	−0.33	0.52	−0.19	−0.002
1.30	−0.09	−0.0000	−0.21	0.33	−0.13	−0.005
1.40	−0.05	−0.0000	−0.14	0.22	−0.09	−0.006
1.50	−0.03	−0.0000	−0.09	0.15	−0.06	−0.006

[a] The contribution to V_c^σ from the cut with branch point at $2M$. See Eq. (23).

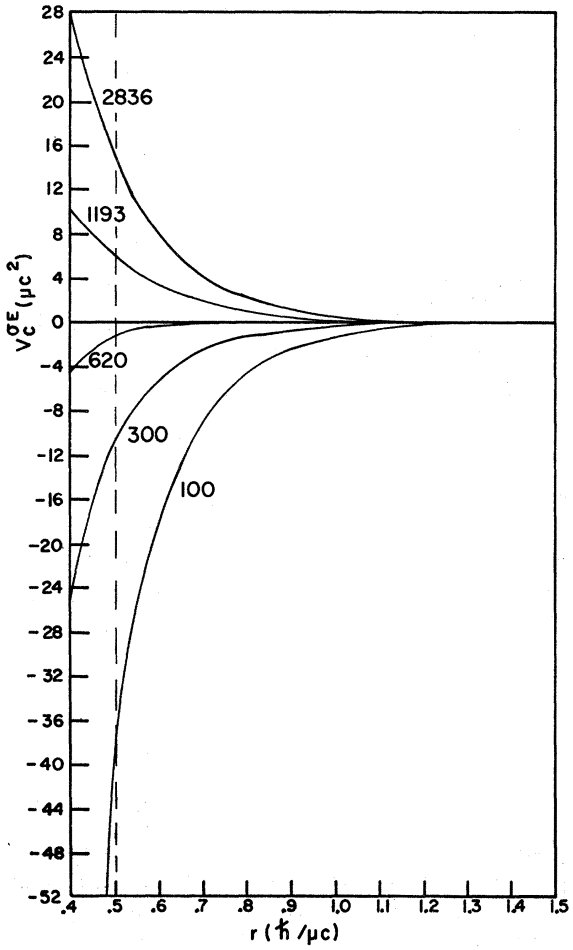

FIG. 12. The σ-exchange central nucleon-nucleon potentials for a broad range of Γ_σ, and $M_\sigma = 765$ MeV. $\Gamma_\sigma = 1193$ MeV corresponds to the Lagrangian of Ref. 6 with $g_A/g_V = 1$, or that of Ref. 10 with $g_A/g_V = 1.37$. The Lagrangian of Ref. 10 with $g_A/g_V = 1$ predicts $\Gamma_\sigma = 2386$ MeV.

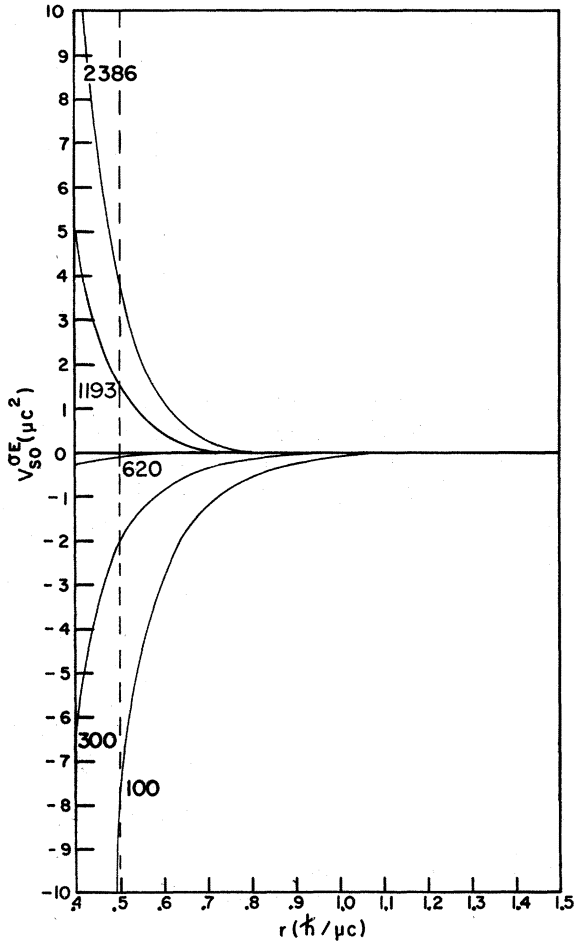

FIG. 13. The σ-exchange spin-orbit potentials for the same cases as Fig. 12.

TABLE II. σ-meson-exchange contribution to the spin-orbit potential. $(g^R_{\pi N})^2/4\pi = 14.4$, $(g_{\sigma N})^2/4\pi = 157.5$, $(g^R_{\sigma N})^2/4\pi = 55.4$ [Eq. (3)], and $(g^R_{\sigma\pi})^2/4\pi = 17.43\mu^2$ corresponding to $\Gamma_\sigma = 620$ MeV. Equation (1) is satisfied.

r (μ^{-1})	V^{σ}_{so} (μ)	ΔV^{σ}_{so} (cut) [a] (μ)	$V^{\sigma\Gamma}_{so}$ (μ)	$V^{\sigma\pi}_{so}$ (μ)	$V^{\sigma\pi\pi}_{so}$ (μ)	$V^{\sigma E}_{so}$ (μ)
0.40	−10.1	0.0783	−7.80	6.24	1.30	−0.261
0.50	−3.51	0.0097	−2.69	2.59	−0.00	−0.104
0.60	−1.35	0.0014	−1.05	1.16	−0.19	−0.084
0.70	−0.55	0.0002	−0.45	0.55	−0.17	−0.068
0.80	−0.24	0.0000	−0.21	0.27	−0.12	−0.049
0.90	−0.11	0.0000	−0.10	0.14	−0.07	−0.034
1.00	−0.049	0.0000	−0.051	0.07	−0.05	−0.023
1.10	−0.023	0.0000	−0.027	0.04	−0.03	−0.015
1.20	−0.011	0.0000	−0.015	0.02	−0.02	−0.010
1.30	−0.005	0.0000	−0.005	0.01	−0.01	−0.003
1.40	−0.003	0.0000	−0.002	0.01	−0.01	−0.002
1.50	−0.001	0.0000	−0.001	0.00	−0.00	−0.001

[a] The contribution to V^{σ}_{so} from the cut with branch point at $2M$. See Eq. (24).

the "pair" potentials. A small change in Γ_σ would improve the cancellation over certain ranges of r. The σ exchange in pion-nucleon scattering [Figs. 6(b) and 6(c)] is indeed adjusted to cancel at zero four-momentum the contribution of Fig. 6(a), which is entirely from the nucleon-antinucleon pair, time-ordered graph in that limit. However, the cancellation between $V^{\sigma E}$ and V^P is affected by Fig. 1(c) and also by being far from zero momentum transfer. For Γ_σ much smaller or larger than 600 MeV the cancellation no longer occurs (although it is still exact for zero-four-momentum pion-nucleon scattering); but for the Weinberg-model width the "pair suppression" effect of σ exchange persists in the nucleon-nucleon interaction.[17] Hence the Weinberg model seems to build in the smooth and slow extrapolation from zero four-momentum needed for direct application of soft-pion results. Perhaps this is related to the asymptotic conditions imposed on tree graphs in the model.[6]

In Figs. 10 to 13 we show the effect of changing Γ_σ on $V^{\sigma E}_c$ and $V^{\sigma E}_{so}$. For $r > 0.4\mu^{-1}$ cancellation is better than 50% of the direct $V^{\sigma\Gamma}$ term for Γ_σ between 300 MeV and the second largest value tried of 1193 MeV (which corresponds to the $g^R_{\sigma\pi}$ of Gell-Mann and Lévy[10] using the reduction factor of g_V^2/g_A^2). For Γ_σ between 540 MeV and 700 MeV the cancellation is better than 90% leading to $V^{\sigma E}$, which do not alter the previously obtained theoretical potential in a major way. The $V^{\sigma E}$ results of Tables I and II, corresponding to the choice $\Gamma_\sigma = 620$ MeV giving optimum cancellation, are displayed in Figs. 10 to 13.

The effect of the addition of the $V^{\sigma E}$ for $\Gamma_\sigma = 620$ MeV to the theoretical potential of Ref. 1 is shown in Figs. 14 and 15. In Ref. 1 the potential is quantitatively similar to the Hamada-Johnston potential.[3] The correction decreases the difference to the Hamada-Johnston potential. $\Gamma_\sigma = 680$ MeV makes the potential more like the Lomon-Feshbach perturbation-theoretic potential of Ref. 16.

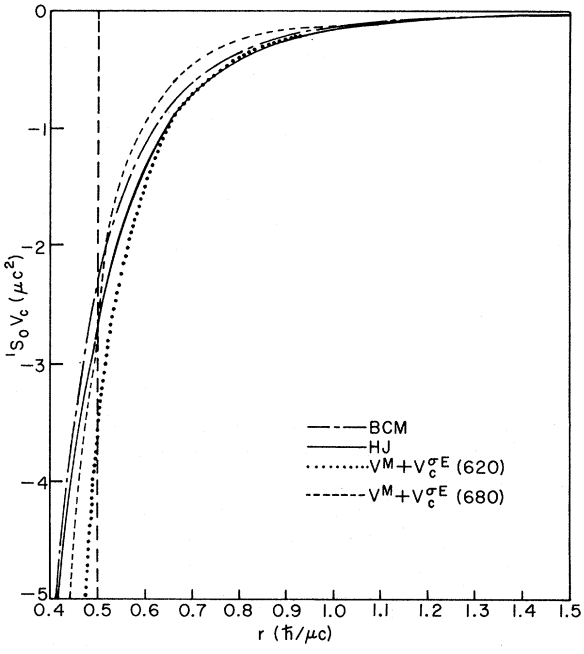

FIG. 14. The effect of adding the σ-exchange central potential (for $\Gamma_\sigma = 620$ or 680 MeV) to the two-pion-exchange potential (TPEP) +one-boson-exchange potential (OBEP) of Ref. 1 is compared with the potentials of Refs. 3 and 16 in the $^1S_0$ state.

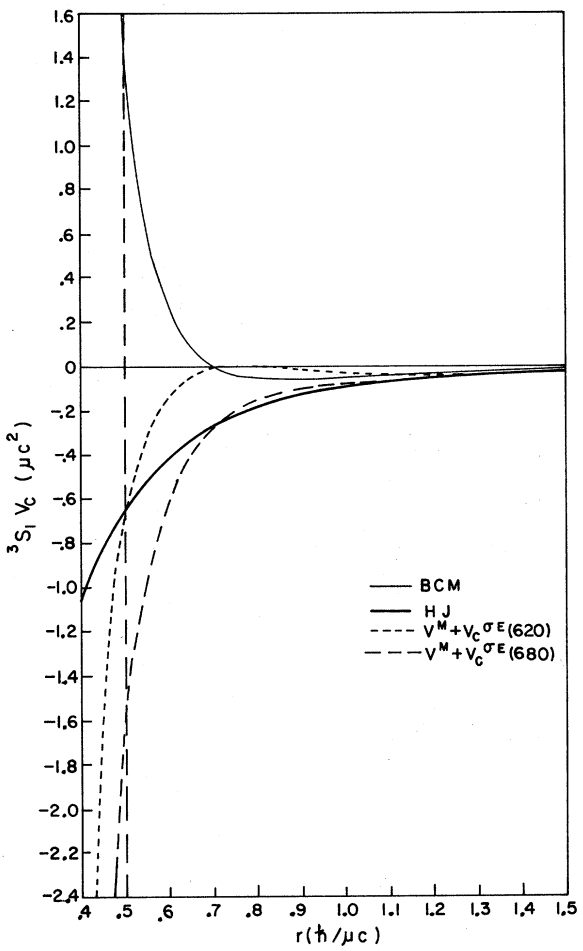

FIG. 15. The comparisons of Fig. 14 are made for the $^3S_1$ state.

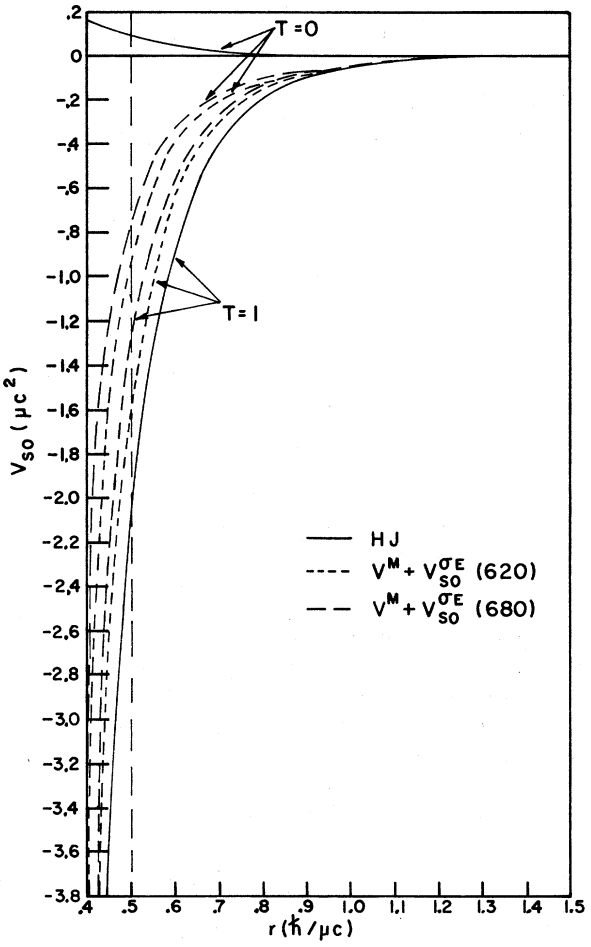

FIG. 16. The effect of adding the σ-exchange spin-orbit potential (for $\Gamma_\sigma = 620$ or 680 MeV) to the TPEP + OBEP spin-orbit potentials of Ref. 1 is compared to the spin-orbit potentials of Ref. 3. The spin-orbit potential of Ref. 16 vanishes for $r > \frac{1}{2}\mu^{-1}$.

The rapidly increasing difference near $r = 0.5\mu^{-1}$ could be absorbed by altering the boundary condition.

The Lomon-Feshbach potential included the nucleon-antinucleon pair terms which apparently compensate for lack of relativistic corrections present in the potential of Ref. 1. With respect to implications for the short-range interaction the Hamada-Johnston potential requires a hard (or nearly hard) core, while the Lomon-Feshbach potential was required in combination with a boundary condition at $r = 0.5\mu^{-1}$. Clearly the new potential obtained here for $r > 0.5\mu^{-1}$ is likely to be consistent with nucleon scattering data, if $\Gamma_\sigma \approx 600$–$700$ MeV.

In terms of the program discussed in Ref. 1 the effect of intermediate-state baryon resonances remains to be calculated. This can be done in terms of the same reduction methods from the relativistic kernel and also using current-algebra restrictions. In the Weinberg model[6] the effects of Δ and P_{11} baryon intermediate states cancel out for zero-four-momentum pion scattering. If the cancellation persists again for the nucleon-nucleon interaction there will be only minor modifications in the low-energy predictions. Energy dependence near resonance-production threshold will, however, be important. We hope to compute this contribution soon.

*This work is supported in part through funds provided by the Atomic Energy Commission under Contract No. AT(30-1)-2098.

†Present address: Arya-Mehr University, Tehran, Iran.

[1]M. Hossein Partovi and Earle L. Lomon, Phys. Rev. D 2, 1999 (1970).

[2]R. Blankenbecler and R. Sugar, Phys. Rev. 142, 1051 (1966); A. A. Logunov and A. N. Tavkhelidze, Nuovo Cimento 29, 380 (1963).

[3]T. Hamada and I. D. Johnston, Nucl. Phys. 34, 382 (1962).

[4]R. Reid, Ann. Phys. (N.Y.) 50, 411 (1968).

[5]H. Kim and Myron Bander, Phys. Rev. D 4, 265 (1971); Earlier $\pi\pi$ phase-shift analyses are reviewed by D. Morgan and J. Pišút, in *Springer Tracts in Modern Physics: Ergebnisse der Exakten Naturwissenschaften*, edited by G. Höhler (Springer, Berlin, 1970), Vol. 55.

[6]Steven Weinberg, Phys. Rev. 177, 2604 (1969).

[7]J. M. Charap and M. J. Tausner, Nuovo Cimento 18, 316 (1960); G. W. N. Cottingham and R. Vinh Mau, Phys. Rev. 130, 735 (1964).

[8]H. Goldberg, Phys. Rev. 154, 1558 (1967); Stanley C. Hirschi, Ph.D. dissertation, M.I.T., 1971 (unpublished).

[9]Steven Weinberg, Phys. Rev. Letters 17, 168 (1966).

[10]M. Gell-Mann and M. Lévy, Nuovo Cimento 16, 705 (1960).

[11]Steven Weinberg, Phys. Rev. Letters 18, 188 (1967).

[12]Stephen L. Adler, Phys. Rev. 137, B1022 (1965).

[13]The same numerical approximation was used in Ref. 1 to obtain the form for the quantity R described after Eq. (4.17). Inclusion of off-mass-shell terms in the expansions of $\vec{p}$, $\vec{p}'$, and W would add to D_2 [Eq. (4.18)] the quantity $\frac{1}{4}(\xi^2-\zeta^2)\Delta^2$. It is numerically unimportant because it is positive; when it is large it pushes the Δ pole in Eq. (4.31) far out, exponentially decreasing the contribution so that it is negligible for $r > \frac{1}{2}\mu^{-1}$. Similar effects permit the on-shell approximation in the present case.

[14]C. Lovelace, Phys. Letters 28B, 264 (1968).

[15]A. Klein, Phys. Rev. 90, 1101 (1953).

[16]Earle L. Lomon and Herman Feshbach, Ann. Phys. (N.Y.) 48, 94 (1968).

[17]For no value of Γ_σ is the Adler condition represented by a momentum-transfer-independent term such as assumed by G. E. Brown and J. W. Durso, Phys. Letters 35B, 120 (1971). For $\Gamma_\sigma = 620$ MeV the momentum-transfer dependence is small for $|t| < 4\mu^2$.

PHYSICAL REVIEW D VOLUME 5, NUMBER 5 1 MARCH 1972

Threshold Relations for Inelastic Neutrino-Nucleon Interactions

Jean Cleymans* and Rudolf Rodenberg
III. Physikalisches Institut, Aachen, Germany
(Received 12 October 1971)

Threshold relations, following from scaling and duality, are obtained for inelastic neutrino-nucleon interactions. Reasonable agreement with existing experimental data is found. It is noticeable that some of the relations are in disagreement with predictions from the parton model.

I. INTRODUCTION

It has become clear recently that there exists evidence for duality and scaling in inelastic electron-proton scattering.[1,2] In particular, the threshold relations, discovered by Bloom and Gilman,[1] are very close to the experimental data. At present it is not clear whether the data on the neutron-to-proton ratio converge to the Bloom-Gilman prediction or if they go to zero.[3] If the second case turns out to be correct, almost all presently existing models are in trouble. Because of the present uncertainty in the data we will not consider seriously this eventuality.

As was pointed out by Llewellyn Smith[4] the predictions following from duality and scaling are not always consistent with those following from the parton model with spin-$\frac{1}{2}$ constituents.[5,6] It is therefore of great interest to find further tests of duality in inelastic form factors. To this end we have turned our attention to deep-inelastic neutrino-nucleon scattering where new experimental data are expected to come out in the near future.

The plan of this paper is as follows: In Sec. II we fix our notations, in Sec. III we review the fundamental work of Bloom and Gilman,[1] in Sec. IV we extend the results of their work to inelastic neutrino-nucleon interactions. In Sec. V we present a discussion of the results.

II. NOTATION

The metric we choose is $(+---)$. All our states will be normalized as

$$\langle \vec{p}\,|\,\vec{p}\,'\rangle = (2\pi)^3 2E\delta^3(\vec{p}-\vec{p}\,').$$

The kinematics for inelastic electron-proton scattering are depicted in Fig. 1.

k: four-momentum of incoming electron,